Failure Morphologies of Cyclically Oxidized ZrO_2-Based Thermal Barrier Coatings

James A. Nesbitt, Dongming Zhu*, Robert A. Miller and Charles A. Barrett

NASA Glenn Research Center
Cleveland, OH 44135

* U.S. Army Research Laboratory
Cleveland, OH 44135

Abstract

Advanced and baseline thermal barrier coatings (TBC's) were thermal cycle tested in air at 1163°C until delamination or spallation of the ceramic top coat. The top coat of the advanced TBC's consisted of ZrO_2 with various amounts of Y_2O_3, Yb_2O_3, Gd_2O_3, or Nd_2O_3 dopants. The composition of the top coat of the baseline TBC was ZrO_2-8wt.%Y_2O_3. All top coats were deposited by air plasma spraying. A NiCrAlY or NiCoCrAlY bond coat was deposited by low pressure plasma spraying onto a single-crystal, Ni-base superalloy. The TBC lifetime for the baseline coatings was approximately 190 cycles (45 minutes at 1163°C per cycle) while the lifetime for the advanced coatings was as high as 425 cycles. The fracture surfaces and sample cross sections were examined after TBC failure by SEM and optical microscopy, and the top coats were further examined by x-ray diffraction. These post-test studies revealed that the fracture path largely followed splat boundaries with some trans-splat fracture. However, there were no obvious distinguishing features which explained the difference in TBC lifetimes between some of the advanced and baseline coatings.

Introduction

Thermal barrier coatings (TBC's) have undergone significant research and development for advanced aeronautic gas turbine applications over the past several decades (Ref 1,2). TBC's, which consist of a ceramic top coat and metallic bond coat, permit increased engine efficiency through higher gas temperatures without increased component temperatures, or extended component life via lower component temperatures. Advanced, 2nd generation TBC's have been the focus of recent studies at the NASA Glenn Research Center (GRC) with a goal to reduce the thermal conductivity of the ceramic top coat. TBC's with lower thermal conductivities will allow even higher gas temperatures, and thereby higher engine efficiencies, at constant component temperatures. However, as the conductivity decreases, the surface temperature of the ceramic top coat increases promoting sintering of the ceramic top coat. Sintering can result in a decrease in coating durability or an increase in the coating thermal conductivity. Hence, a secondary goal of the studies at NASA GRC is to retain the reduced thermal conductivity during high temperature exposures while maintaining or exceeding the durability of current state of the art TBC's.

The approach being taken at the NASA GRC to develop advanced TBC's is to dope ZrO_2 -Y_2O_3 top coats with various rare earth oxides (Gd_2O_3, Nd_2O_3 and/or Yb_2O_3)[Ref 3]. The thermal conductivity and sintering resistance of these coatings is being evaluated with a high heat-flux laser rig [Ref 4]. Although the thermal conductivity of numerous coatings has been measured in laser tests for durations up to 20 hours, it is impractical to perform

extended durability testing of the large number of coating compositions, well in excess of 40, in the laser rig. Hence, durability screening testing of one or two samples of each coating composition is being performed using automated cyclic oxidation furnace rigs which thermally cycle coated samples in an oxidizing environment. Coated samples were cyclically oxidized until ceramic top coat failure by cracking or delamination, for times reaching several hundreds of hours. The purpose of the present study was to examine the microstructural and morphological changes in select coatings after coating failure. Comparisons were made to baseline coatings without rare earth additions.

Experimental

Four samples with advanced top coat compositions which exhibited cyclic oxidation lifetimes much less than, similar to, and much greater than the average baseline lifetimes were selected for study. The cyclic oxidation lifetime (i.e., the coating lifetime or time to coating failure) was defined as the time when approximately 20% of the ceramic top coat had spalled or was obviously delaminated. The thermal barrier coating system for all coatings, advanced and baseline, consisted of an air plasma sprayed (APS) ceramic top coat and a low pressure plasma sprayed (LPPS) NiCrAlY or NiCoCrAlY bond coat deposited on one side of a disk-shaped substrate of single crystal René N5 Ni-base superalloy. The dimensions of the substrate disk were 25.4 mm diameter by 3.2 mm thick. The thickness of the Ni(Co)CrAlY bond coat was nominally 120 microns and the thickness of the top coat was nominally 180 microns. The nominal composition of the baseline top coat[1] was ZrO_2-8wt.%Y_2O_3, commonly referred to as 8YSZ (8 wt.% Y_2O_3 stabilized ZrO_2). The spray parameters for the LPPS bond coats were identical for all samples. Likewise, the spray parameters for the APS ceramic top coats, for both the baseline and the advanced coatings, were identical.

The advanced coatings varied in dopant content, including Y_2O_3, from 12 to 31 wt.%. The powders were fabricated by spray drying powders of the desired composition followed by twice spraying the powders in the plasma torch to react, homogenize and spheroidize the alloy powders. Coating designations, total dopant content and top coat thickness are given in Table I.

Table 1 Coating Designations, Total Dopant Content and Coating Life

Coating Designation	Total Dopant Content (wt%) [mol%] (dopants)*	Top Coat Thickness (microns)	Coating Life (cycles)	Total Elevated Exposure (cycles, [hrs])
Base-8	8 [4.5] (Y)	180	188 ± 25 **	170 [127.5], 190 [142.5], 220 [165]
ADV-12	12 [5.5] (Y,Gd,Yb)	188	225 ± 5‡	230 [172.5]
ADV-26A	26 [13.5] (Y,Nd,Yb)	190	185 ± 5‡	190 [142.5]
ADV-26B	26 [13.5] (Y,Gd,Yb)	190	425 ± 5‡	430 [322.5]
ADV-31†	31 [16] (Y,Nd,Yb)	183	25 ± 5‡	30 [22.5]

* Y, Gd, Nd and Yb refer to the oxides Y_2O_3, Gd_2O_3, Nd_2O_3 and Yb_2O_3

** Average of three samples with lifetimes of 165,185 and 215.

‡ Single sample tested. Uncertainty reflects the 10 cycle inspection period.

† Received NiCoCrAlY rather than NiCrAlY bond coat used on all other samples.

Add relation for patent pending DMC 8/20/02

[1] The top coat powder was Zirspra 9507/46, available from Zircoa Corp.

Cyclic oxidation testing was performed in an automated cyclic furnace rig capable of testing up to twelve samples at a time. The furnace consists of symmetric heating elements surrounding 6 alumina vertical tubes. Coated samples were automatically lowered into or raised from the center of the furnace for preset heating and cooling times. In this study, one cycle consisted of a 45 minute elevated temperature exposure followed by a minimum 15 minute cooling period. The elevated temperature exposure was 1163°C (2125°F) which was reached in approximately 2 minutes. The 15 minute cooling period allowed the samples to cool to approximately 120°C. The temperature variation between the six tubes at the center of the furnace was ±3°C. The samples were inspected after every 10 cycles which resulted in an uncertainty of ±5 cycles in determining the failure of the top coat. Upon observed coating failure, the samples were removed from the furnace. The coating lifetimes, in cycles, as well as the total time at the elevated temperature, is given in Table I. After testing, the ceramic top coats were examined by x-ray diffraction and the fracture surfaces between the bond coat and top coat were examined by scanning electron microscopy (SEM) and energy dispersive spectroscopy (EDS). Following examination of the fracture surfaces, the samples were sectioned and polished and the cross sections examined by SEM, EDS and optical microscopy (OM).

Results and Discussion

Bond Coat and Thermally Grown Oxide (Alumina): The NiCrAlY and NiCoCrAlY bond coats contained predominately the $\gamma+\beta$ phases (γ-Ni solid solution FCC structure, β-NiAl structure) where the β phase acts as an Al reservoir. During the elevated temperature exposures, Al diffuses to the bond coat/top coat (BC/TC) interface and is selectively oxidized to form a protective Al_2O_3 layer. This layer is commonly referred to as the "thermally grown oxide," or TGO. The diffusion of the Al results in the recession of the β phase away from the BC/TC interface. At the same time that Al diffuses to form and grow the TGO, Al and also Cr diffuse into the substrate while substrate elements diffuse into the coating. As a result of this interdiffusion, the β phase in the bond coat recedes from the substrate while the γ' phase in the substrate recedes from the bond coat (Figure 1). Eventually the β phase is depleted while new phases form in the so-called "Diffusion Zone" near the bond coat/substrate interface (Figure 2). These new phases were rich in refractory elements (Cr, W, Re) from the substrate and are commonly identified as topologically close packed (TCP) phases. Total depletion of the β phase depends on the bond coat thickness but appeared complete after approximately 180-200 cycles, the average lifetime for the baseline samples as well as for two of the advanced TBCs. As Al was selectively oxidized to form the TGO, the Cr concentration in the bond coat near the TGO increased. This increase resulted in the formation of small α-Cr particles in the bond coat below the TGO, as shown in Figure 2.

The NiCoCrAlY bond coat used with the ADV-31 top coat was an attempt to see if the addition of Co, substituting for a small amount of the Ni, would improve the cyclic oxidation lifetime of these coatings. However, after cyclic oxidation testing, it was observed that the bond coat did not form a good bond with the substrate (note the dark line of porosity near the bond coat/substrate interface in Figure 1). As a result, oxidation penetrated this interface and caused the bond coat to delaminate from the substrate. The delamination of the bond coat also caused the observed premature delamination of the top coat. Consequently, the short lifetime of the top coat can be attributed to the poor bonding between the bond coat and substrate and not as a result of the ceramic top coat composition. Hence, further analysis of the top coat will not be reported in this paper.

The alumina TGO growing on the bond coat of the baseline alloys appears to be more convoluted and to have penetrated into the bond coat more so than that on the advanced coatings (Figure 3). This internal oxidation is likely the result of porosity in the coating following the plasma spraying since the composition of each of the bond coats shown in Figure 3 was identical (Ni-22Cr-10Al-1Y wt%). Porosity that is interconnected or linked to the surface could produce the observed morphology. Smaller amounts of unoxidized porosity are shown in Figure 3b. However, the processing variations that could have resulted in interconnected porosity in the baseline alloys are unclear since all measured variables were identical. It was also apparent that the thickness of the bond coat on the baseline alloys (Figure 3a) was less than that for the advanced alloys (Figures 3b-d). The bond coat appears relatively unchanged after approximately double the thermal exposure (compare Figures 3c and d). Although the BC/TC interface was far from planar, the thickness of the TGO was measured at numerous locations (Figure 4a) on each of the samples. The scale appeared to grow approximately parabolic, as shown in Figure 4b. As expected, in both the advanced and baseline bond coats, Ni yttrides were evident in the bond coat (Figure 4a) and numerous Y-enriched regions, which imaged brighter than the alumina, were observed throughout the TGO (Figure 4c). Although too small for analysis, the Y-enriched regions were possibly the $Y_3Al_5O_{12}$ (YAG) phase. Similarly, transient Ni- and Cr-containing oxides were observed between the TGO alumina and the top coat (Figure 5a). At high asperities, such as an unmelted bond coat powder particle, the entire particle was often oxidized (Figure 5b).

Ceramic Top Coat: Typically, large sections of the ceramic top coat fractured and delaminated from the bond coat. This behavior allowed both fracture surfaces to be examined, viewing the underside of the top coat and viewing down towards the bond coat. These two surfaces will be referred to as the top coat fracture surface and the bond coat fracture surface. Examining either fracture surface using back scattered electron imaging (BSE) allowed the top coat and TGO to be easily distinguished. Pieces of the top coat were also examined by x-ray diffraction to determine the phases present in the top coat at the time of failure.

1. Baseline Alloys. In the baseline alloys, the majority of the fracture path passed through the top coat with approximately 30% passing through or exposing the TGO. Figure 6a shows the bond coat fracture surface. Most of the bright regions are ceramic top coat. A small portion of the bright regions are exposed bond coat metal. At higher magnifications of the bright, top coat regions, it is clear that the fracture path has largely followed the splat boundaries of the sprayed ceramic top coat (Figure 6b). Less numerous regions where the fracture path appeared to cut through the top coat splats is shown in Figure 6c. Regions where the fracture path primarily followed top coat splat boundaries but cut through the alumina scale exposing a bond coat asperity are easily seen in the secondary electron image (SEI) and BSE image in Figure 7. In contrast to the normal splat powder particle morphology, large irregularly-shaped grains were apparent in various regions of the fracture surface (Figure 8). Comparison of EDS spectra of these large-grained regions and the smooth splat regions did not show any difference.

BSE imaging the top coat fracture surface revealed about half the amount of TGO alumina attached to the top coat (Figure 9a). The difference in the amount of TGO (~30% dark in Figure 6a vs 16% in Figure 9a) can be explained if the fracture path cuts through asperities in the bond coat but follows the TGO/top coat interface for short distances around those asperities. In this manner, more of the TGO would be exposed in the bond coat fracture surface than on the top coat fracture surface. Many of the dark TGO regions appear circular (Figure 9a). A magnified view of one of those regions (Figure 9b) indicates that the fracture path cut across a circular asperity revealing an alumina ring filled with Ni

and Cr oxides. It is expected that these asperities are either bond coat mounds, such as shown in the top center of Figure 3b, or large unmelted powder particles, such as shown in Figure 5b. There was significant evidence on the top coat fracture surface that the fracture path primarily followed intersplat boundaries.

The x-ray diffraction spectra for the Base-8 coating after 220 cycles is shown in Figure 10. As previously reported, the structure of the coating is primarily tetragonal with a small amount of monoclinic (see inset in Figure 10a) (Ref 5). Both the (400) and (004) tetragonal peaks are clearly shown in Figure 10b. Little change is expected in the crystal structure with extended exposures at the current test temperature of 1163°C (Ref. 6).

2. Advanced Alloys. BSE imaging the bond coat fracture surface indicated an amount of exposed TGO (~26% and 34%) for the ADV-12 and ADV-26A alloys (Figure 11), similar to that of the baseline alloys (30%, Figure 6a). The amount of TGO attached to the underside of the top coat for these two alloys (14% and 4%) was somewhat lower than that for the baseline(16%, Figure 9a). However, like the baseline alloys, many of the TGO regions on the top coat fracture surface appeared circular (Figures 9, 11b, 12b). In contrast, the amount of TGO on the bond coat fracture surface of ADV-26B, with approximately twice the number of cyclic exposures, was significantly higher (~56%) while the TGO attached to the underside of the top coat (the top coat fracture surface) was similar to that for the other alloys (10%) (Figure 13).

On each of the advanced coatings, there was significant evidence of fracture along splat boundaries when viewing either the bond coat or top coat fracture surfaces (Figure 14). However, in each of the advanced coatings, there were also regions with the irregular, shaped oxide structures easily distinguished from the smooth, splat morphology (Figure 15) This irregular shaped morphology was somewhat similar to that observed in the baseline alloys (Figure 8b). Comparison of the EDS spectra from the irregular morphology and the smooth splat morphology gave some indication that the irregular shaped oxide was higher in dopant content, particularly Yb, however, this enrichment was small and wasn't observed uniformly in all regions examined. Further analysis by electron microprobe of the polished cross-sections might confirm any compositional inhomogeneity.

The x-ray diffraction spectra for the advanced coatings are shown with the baseline coatings in Figure 10. Increasing the dopant concentration from the baseline concentration of 8 to 12 eliminates the monoclinic phase but maintains the tetragonal structure. However, increasing the dopant concentration to 26% results in the stabilization of the cubic rather than the tetragonal structure. Since the ADV-12 and ADV-26A coatings have similar cyclic lifetimes (225 and 185) but different crystal structures (tetragonal and cubic), it appears that the crystal structure, at least for this range of dopant concentrations, does not have a major effect on the coating lifetime. Similarly, ADV-26A and ADV-26B coatings both possess cubic crystal structures, yet the ADV-26B coating lifetime was twice that of the ADV-26A. Since the bond coats were nearly identical for both coatings (sprayed at the same time), the only obvious difference is that the ADV-26A coating contains Nd_2O_3 as one of the dopants while Gd_2O_3 replaces the Nd_2O_3 in the ADV-26B coating.

Summary

In summary, for the three advanced alloys with the NiCrAlY bond coat, there was no significant difference in the appearance of the TGO alumina scale. Although there was significant TGO growth within the NiCrAlY bond coat on the baseline alloys, this internal oxide growth did not appear to have had a significant effect on the TBC life since the coating life of two advanced alloys, devoid of the internal oxide growth, was similar to that

of the baseline alloys. If the internal oxidation was the result of interconnected porosity in the bond coat, the cause of the porosity was unclear. Although convoluted, the TGO scale appeared to thicken parabolically with time.

X-ray diffraction analysis of each top coat indicated that the differences in the crystal structures could not account for the long lifetime of the ADV-26B coating. Likewise, examination of the fracture surfaces for the baseline and advanced coatings did not reveal any obvious cause for the longer lifetime of the ADV-26B coating. Over the range of total dopant concentrations of Y_2O_3+Yb_2O_3+(Gd_2O_3,Nb_2O_3) from 8 to 26 wt.%, there were no obvious distinguishing characteristics in the appearance of the top coat fracture morphology. The fracture path appeared to pass largely along splat boundaries, but with some trans-splat fracture. Although the splat morphology was most prevalent, a large-grained, irregularly shaped morphology was observed on both the baseline and advanced coating alloys. There was some indication that these irregularly shaped grains had slightly higher dopant concentrations in the advanced alloys, however, this observation was not consistently observed. For the ADV-31 coating, the premature top coat failure was attributed to the bond coat delamination. The effect of dopant concentrations on the coating lifetime continues to be studied at the NASA GRC.

Acknowledgements

This work was performed under sponsorship of the Space Transportation and Propulsion Office, Propulsion Research & Technology Project (Mark Klem Project Manager) and the Ultra Efficient Engine Technology programs (Robert Draper Program Manager) at the NASA Glenn Research Center.

References

1. Zhu, D. and Miller, R.A., "Thermal Barrier Coatings for Advanced Gas-Turbine Engines", MRS Bulletin, 27, 43-47, 2000.

2. Miller, R.A., Garlick, R.G., and Smialek, J.L., American Ceramic Soc. Bull. 62, 1355 (1983).

3. Miller, R.A., Smialek, J.L., Garlick, R.G., ni Advances in Ceramics: Science and Technology of Zirconia, vol 3, Heuer, A.H. and Hobbs, L.W., Editors, Columbus OH, The American Ceramic Society, 1981, p. 241.

4. Zhu, D. and Miller, R.A., "Thermal Conductivity and Sintering Behavior of Advanced Thermal Barrier Coatigns", Ceramic Sci. Eng. Proc., vol 23, 2002.

5. Zhu, D. and Miller, R.A.,"Low Conductivity and Sintering Resistant Thermal Barrier Coatings," US Patent Application Serial Number 09/904,084, USA.

6. Demasi-Marcin, J.T. and Gupta, D.K. Surface and Coatings Technol., 68/69, 1 (1994).

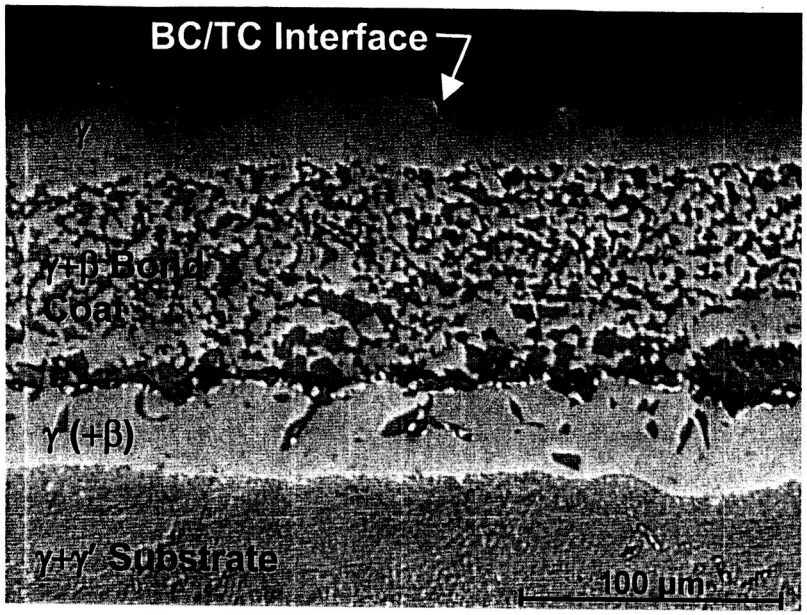

Figure 1. NiCoCrAlY bond coat after 30 cycles (22 hrs) at 1163°C showing the γ+β phases in the bond coat, the β recession away from the bond coat/top coat (BC/TC) interface, and the recession of the γ′ from the BC/substrate interface (ADV-31).

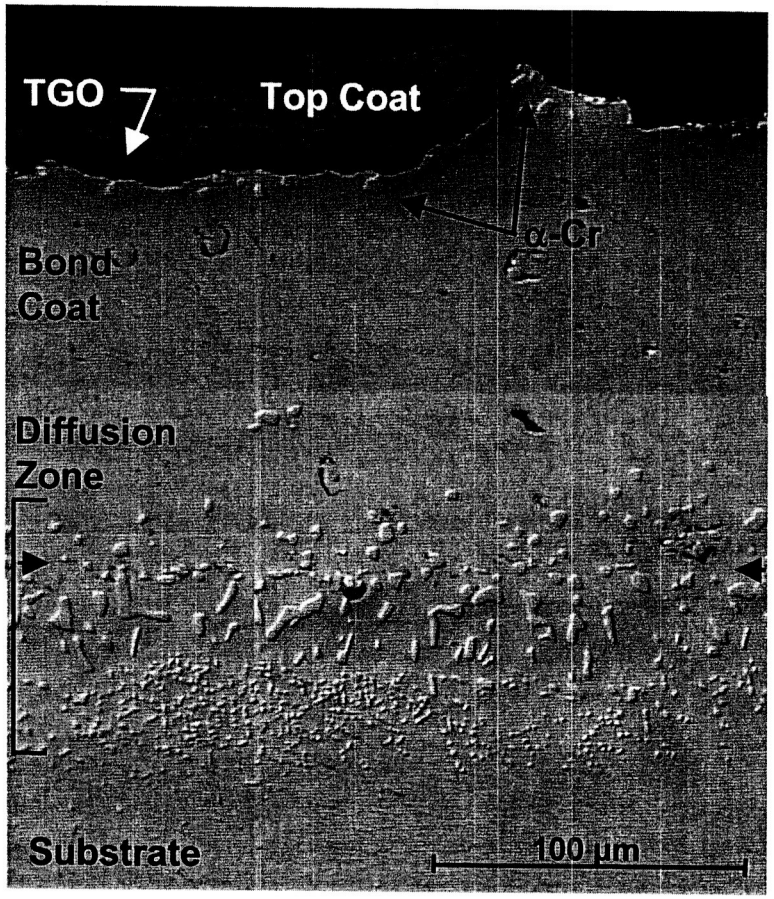

Figure 2. Bond coat after 230 cycles (172 hrs) at 1163°C showing diffusion zone, α-Cr particles near BC/TC interface, TGO alumina layer and some remaining top coat. Short arrows indicate approximate position of original BC/substrate interface.

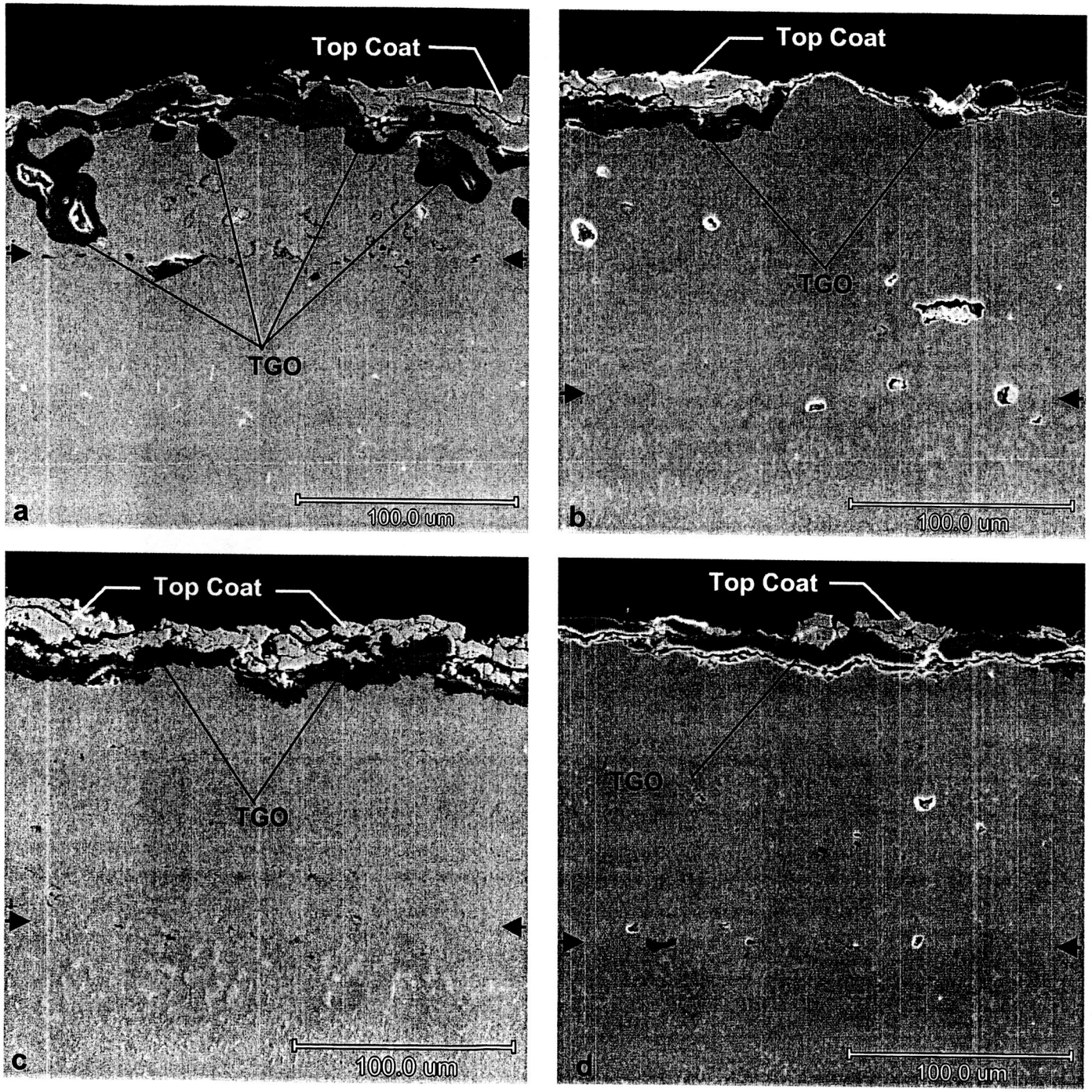

Figure 3. Oxidized bond coats on the (a) Base-8 (190 cycles), (b) ADV-12 (230 cycles), (c) ADV- 26A (190 cycles) and (d) ADV- 26B (430 cycles) coatings. Porosity is apparent in the ADV-12 bond coat and internally oxidized regions in the Base-8 bond coat. Short arrows indicate approximate position of the BC/substrate interface.

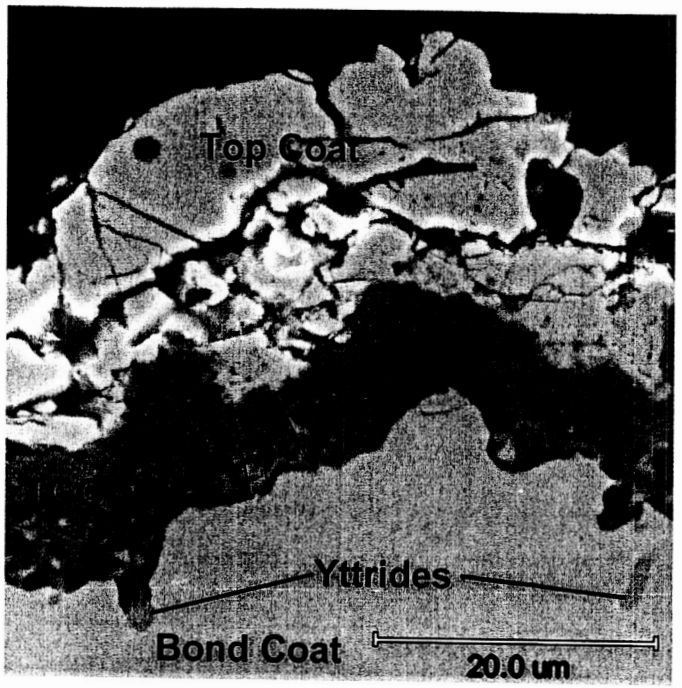

a

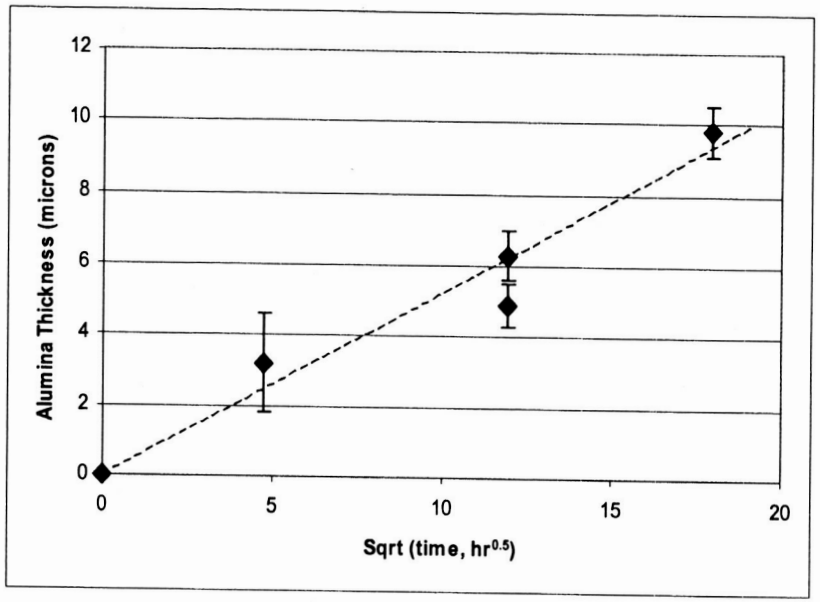

b

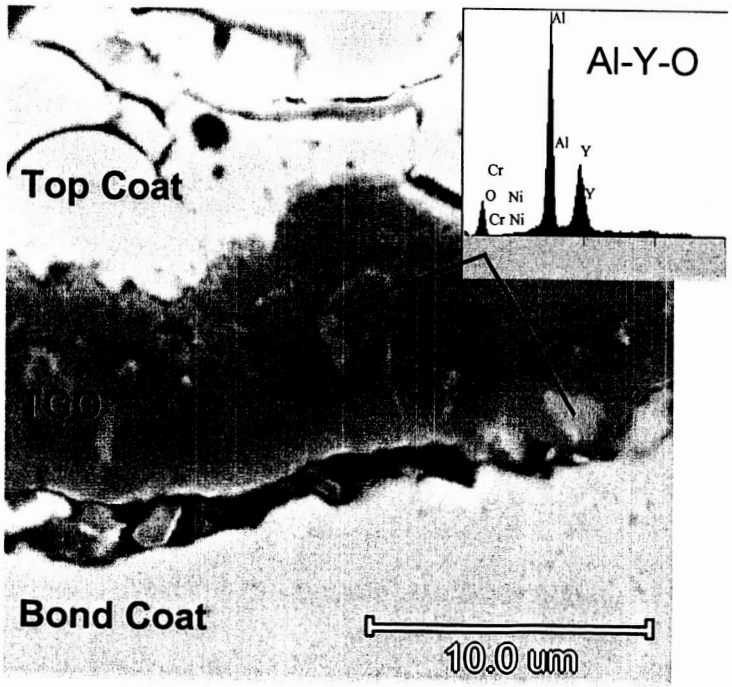

c

Figure 4. (a) Example of TGO alumina thickness measurements (b) TGO thickness plotted against the square root of the total exposure time. (c) Y-enriched regions in the alumina TGO (ADV-12, 230 cycles (172.5 hrs).

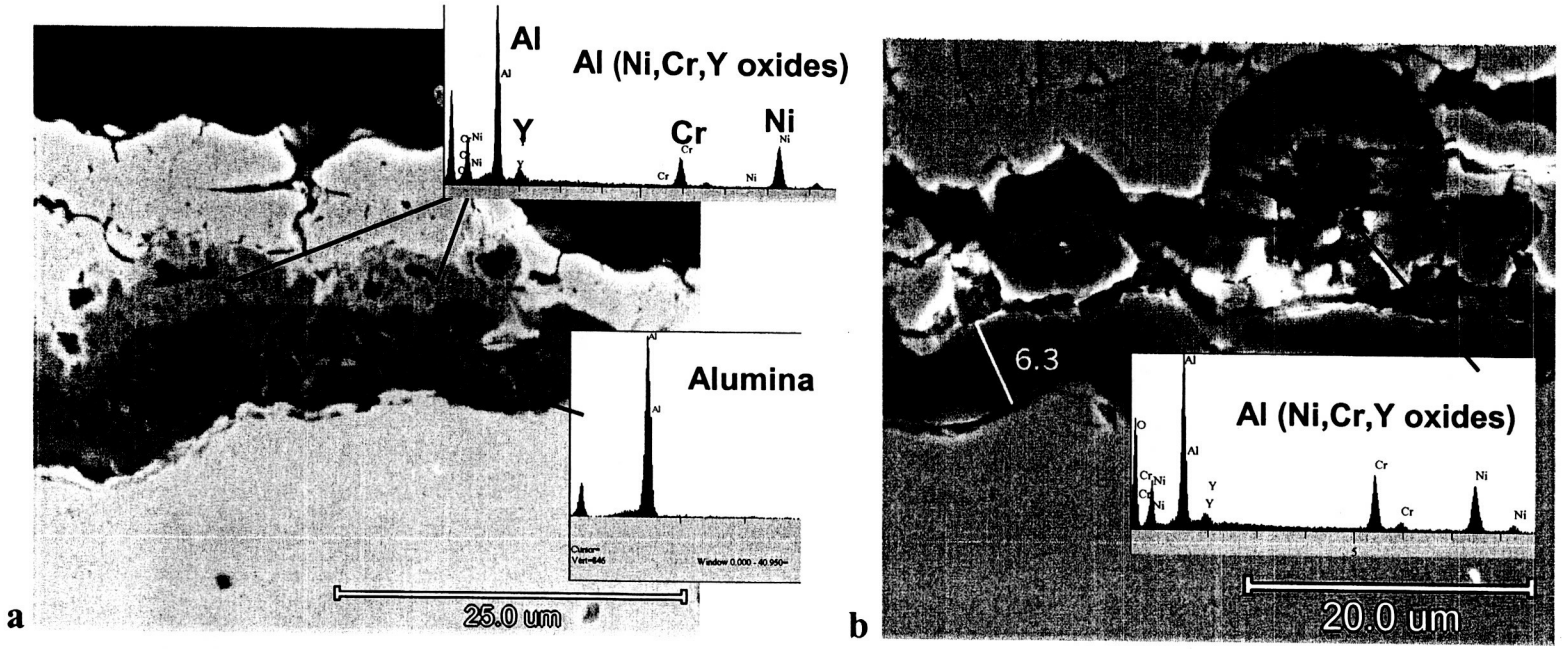

Figure 5. Transient Ni- and Cr-containing oxides above the alumina TGO (a) Base-8, 190 cycles, (b) ADV-12, 230 cycles. (Y-enriched regions are also evident in the TGO.)

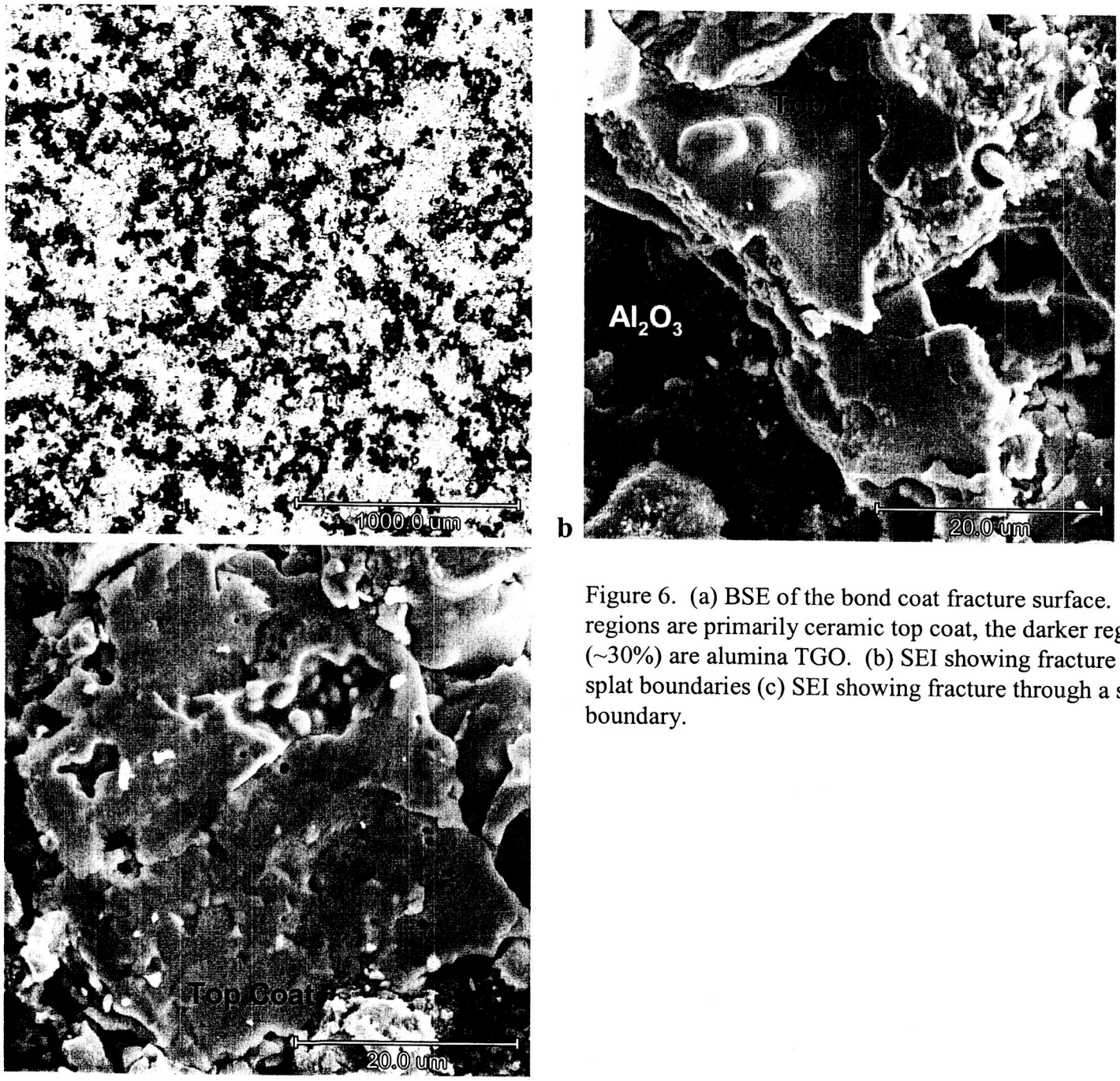

Figure 6. (a) BSE of the bond coat fracture surface. Light regions are primarily ceramic top coat, the darker regions (~30%) are alumina TGO. (b) SEI showing fracture along splat boundaries (c) SEI showing fracture through a splat boundary.

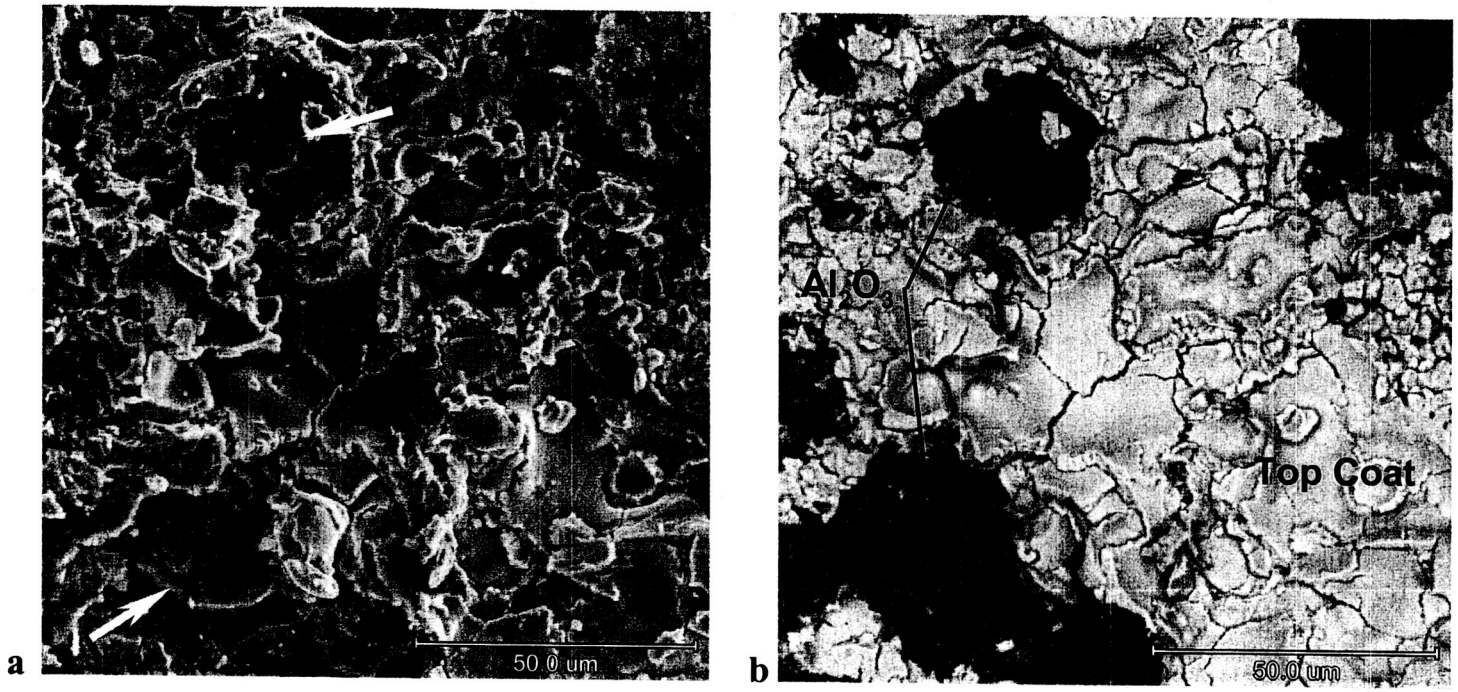

Figure 7. (a) SEI and (b) BSE images of the same location on the bond coat fracture surface on the baseline coatings. Dark regions in (b) are TGO. The BSE image shows that the fracture path cuts through the alumina TGO to expose bond coat asperities (white arrows in **a**). The asperities are oxidized in the current figure since they appear dark in the BSE image (b). Primarily intersplat fracture through the top coat is evident.

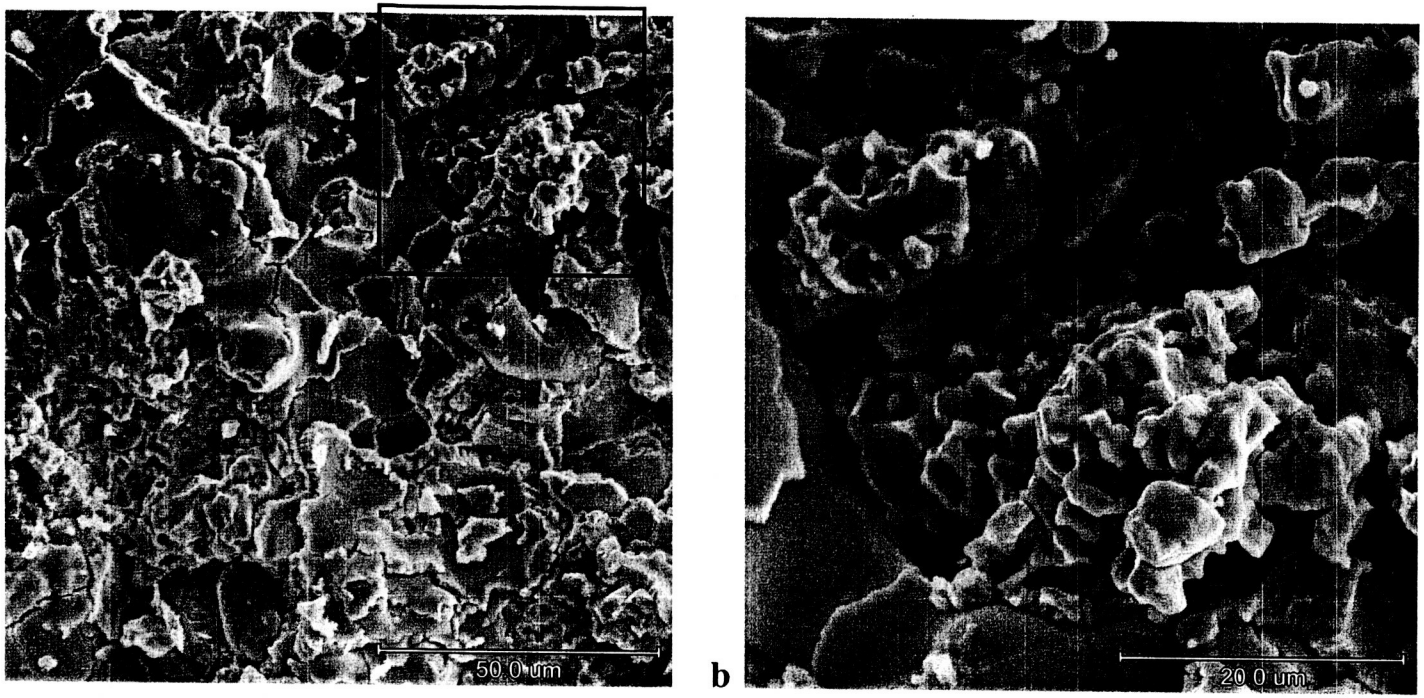

Figure 8. (a) SEI of the bond coat fracture surface showing significant intersplat fracture. BSE image indicates nearly all oxide is zirconia-yttria.. (b) Higher mag of the inset in (a) showing the larger, irregularly-shaped grains (Base-8, 220 cycles).

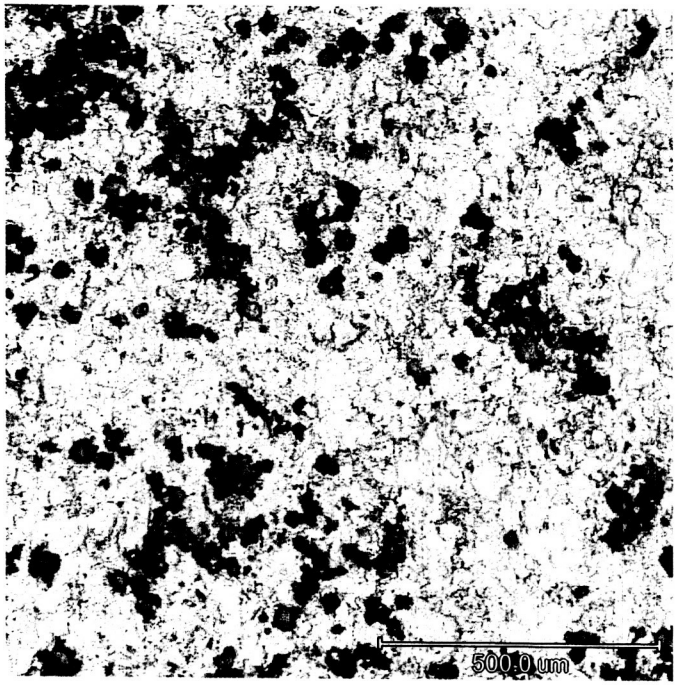

a

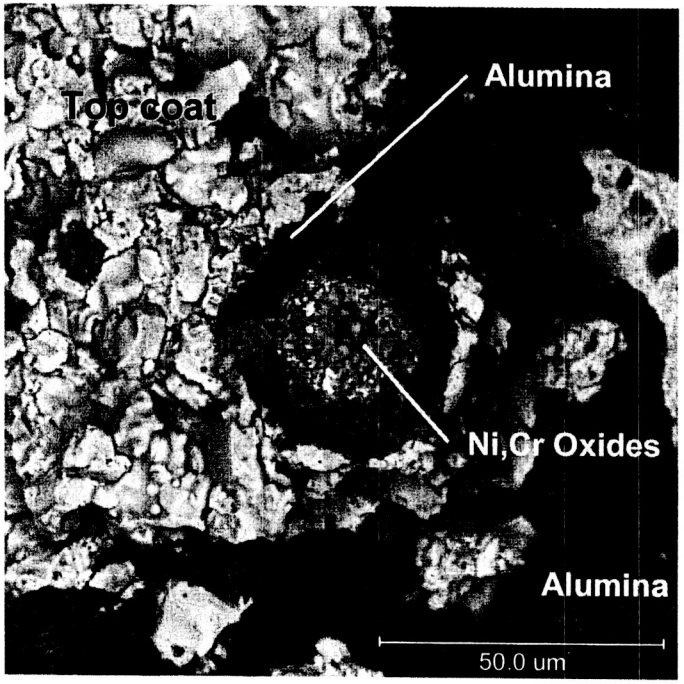

b

Figure 9. BSE image of (a) the top coat fracture surface. Dark regions (~16%) are TGO. (Base-8, 220 cycles) and (b) one of the circular features on the top coat fracture surface. The darkest regions are alumina. Intermediate gray regions are mixed Ni and Cr oxides. The small, bright regions intermixed with the Ni and Cr oxides are Ta-rich oxides (Base-8, 220 cycles).

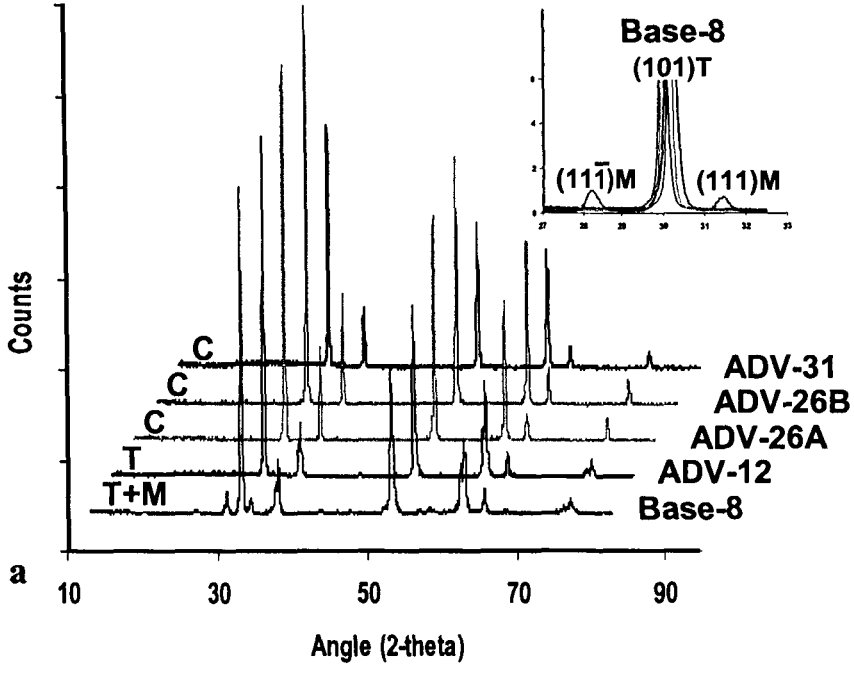

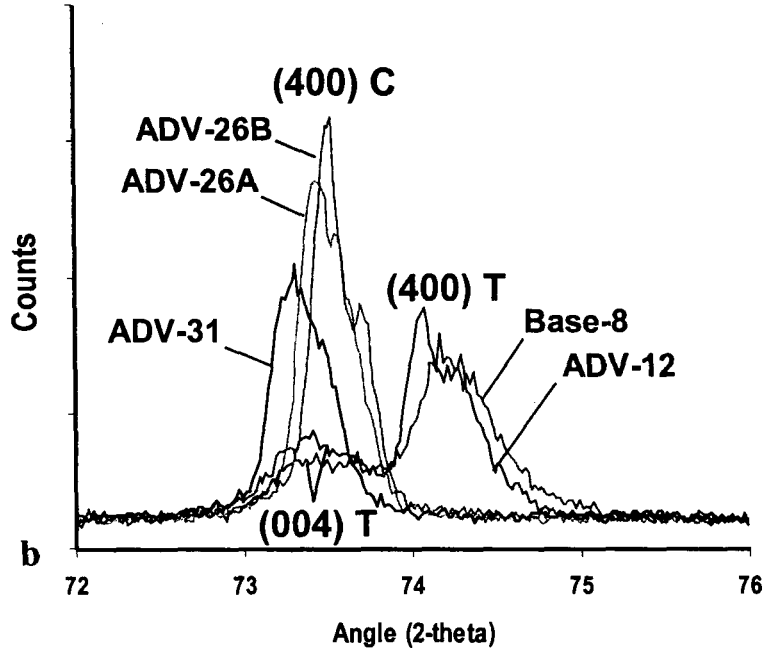

Figure 10. X-ray diffraction peaks of the top coat after coating failure (a) full measured spectra for each coating. The inset shows the monoclinic peaks for the Base-8 coating. (b) Expanded scale showing the tetragonal (400), (004) and cubic (400) peaks. T-tetragonal, M-monoclinic, C-Cubic.

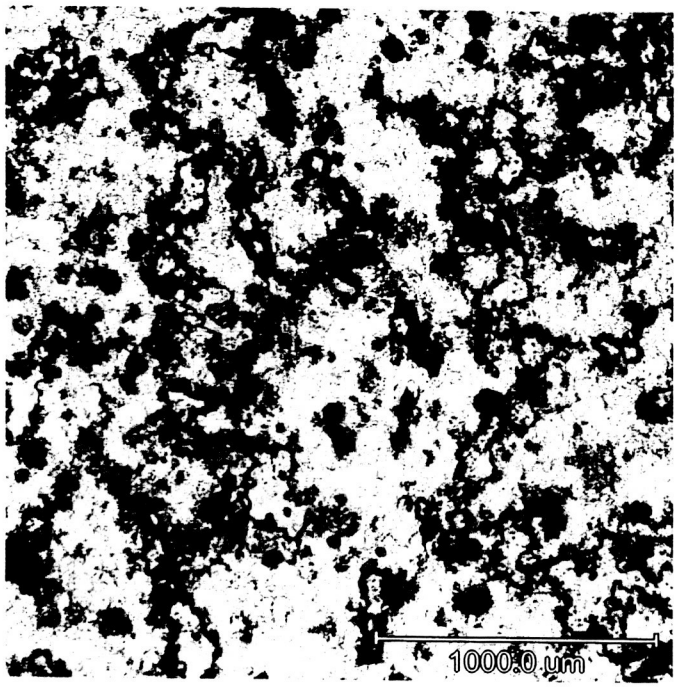

a

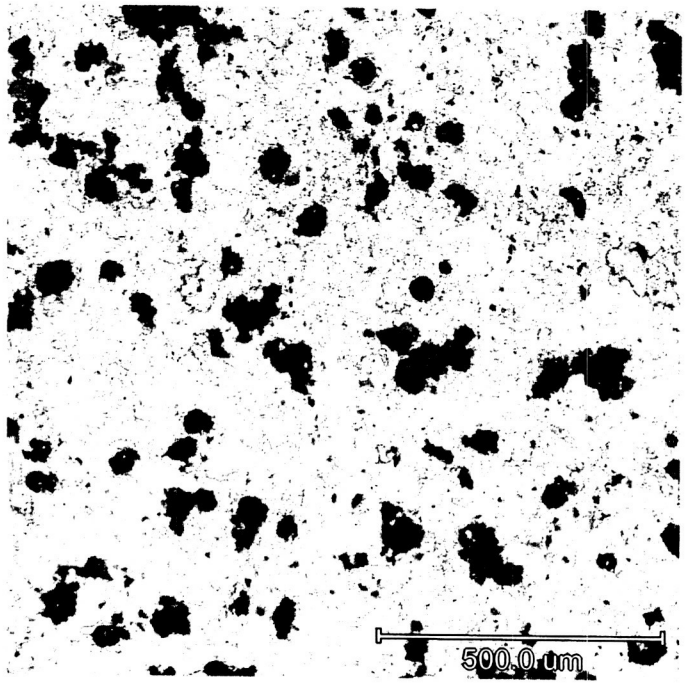

b

Figure 11 BSE image of the (a) bond coat fracture surface and (b) top coat fracture surface (ADV-12, 230 cycles). Dark regions are TGO, approximately 34% in (a), 14% in (b).

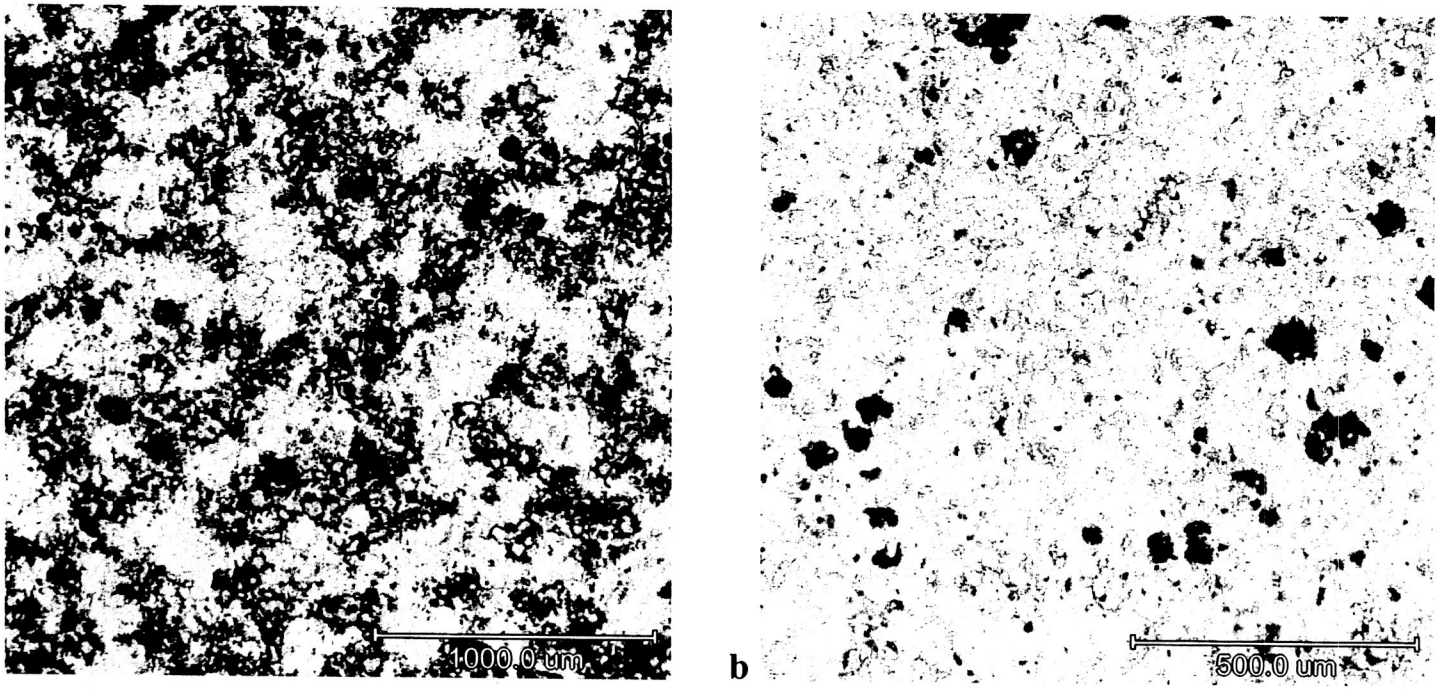

Figure 12 BSE image of the (a) bond coat fracture surface and (b) top coat fracture surface (ADV-26A, 190 cycles). Dark regions are TGO, approximately 26% in (a), 4% in (b).

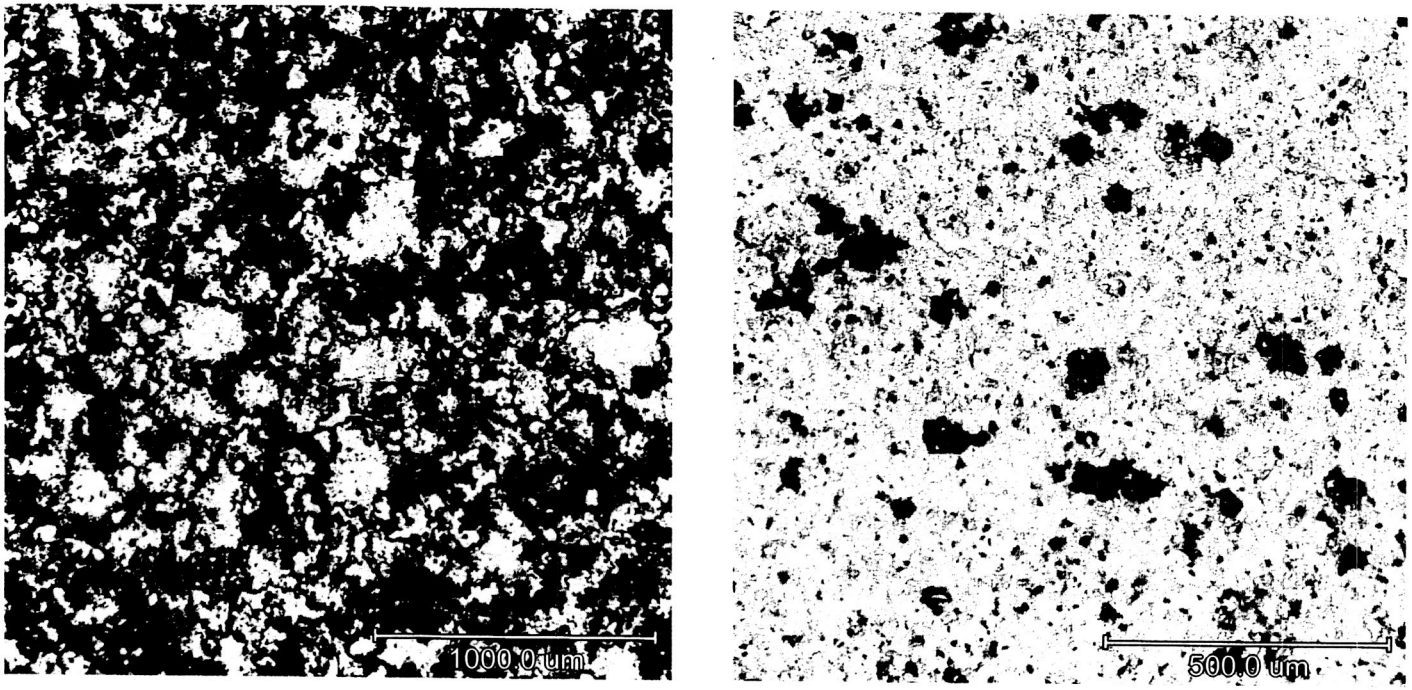

Figure 13 BSE image of the (a) bond coat fracture surface and (b) top coat fracture surface (ADV-26B, 430 cycles). Dark regions are TGO, approximately 56% in (a), 10% in (b).

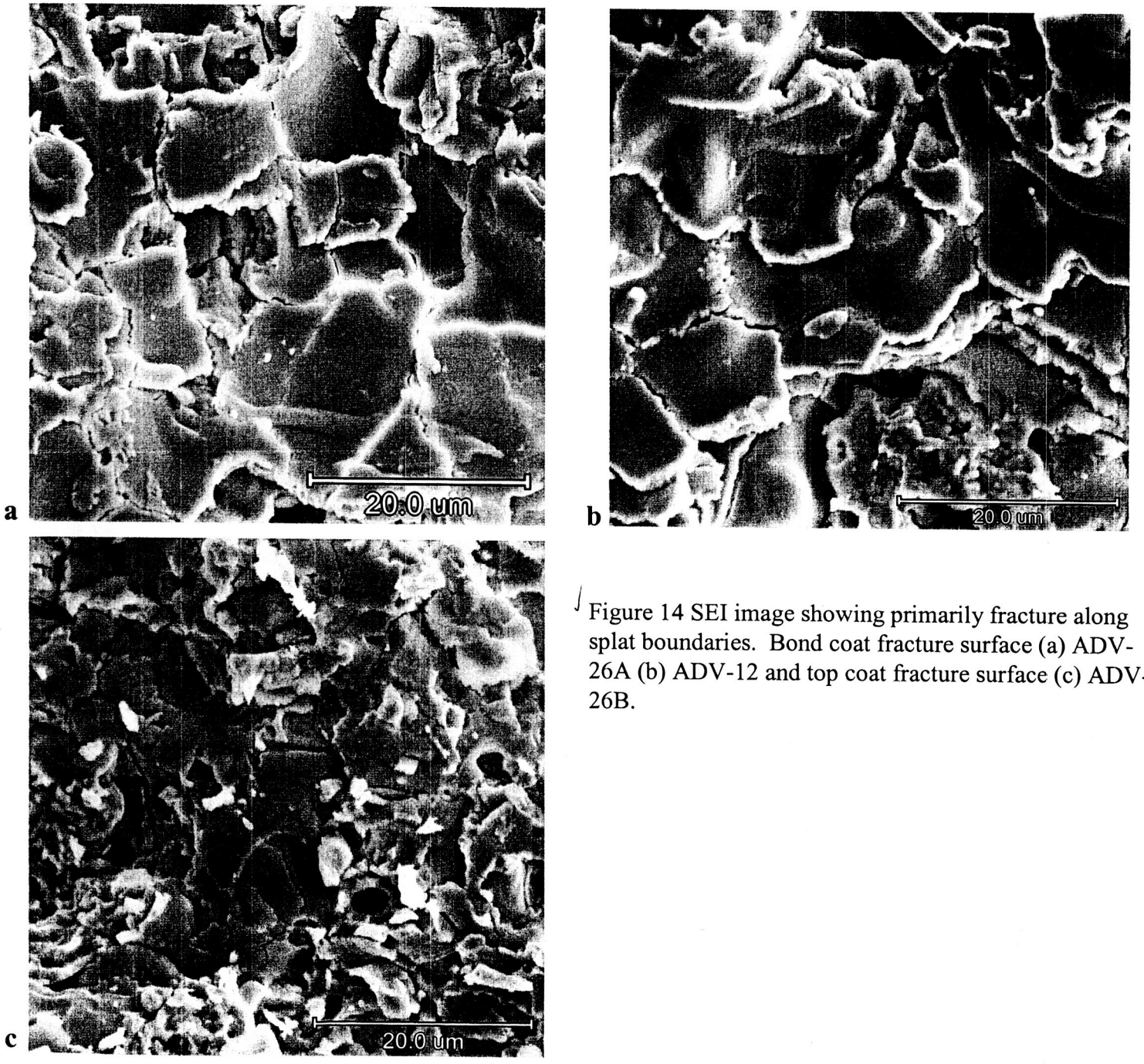

Figure 14 SEI image showing primarily fracture along splat boundaries. Bond coat fracture surface (a) ADV-26A (b) ADV-12 and top coat fracture surface (c) ADV-26B.

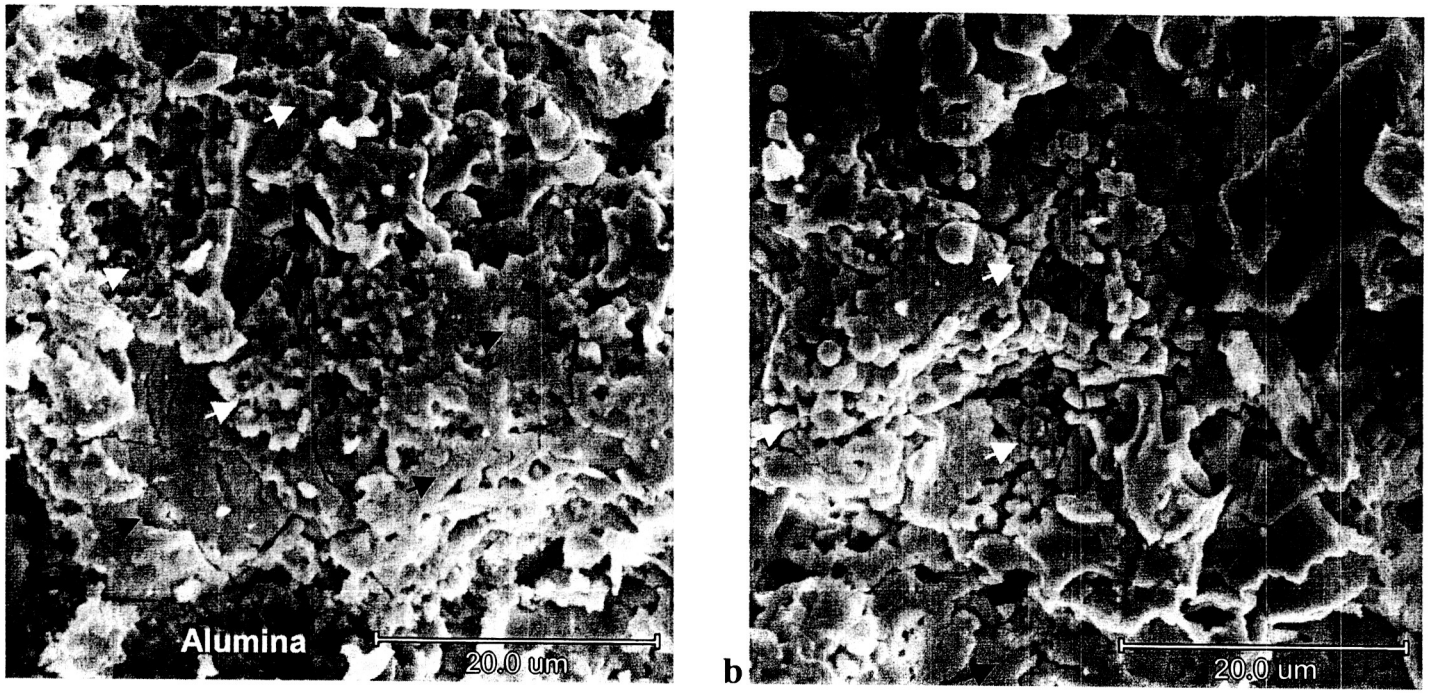

Figure 15 (a), (b) SEI image showing the irregular-shaped oxide structure on the top coat fracture surface of ADV-26A. White arrows indicate the irregular-shaped oxide, black arrows indicate smooth intersplat boundaries.

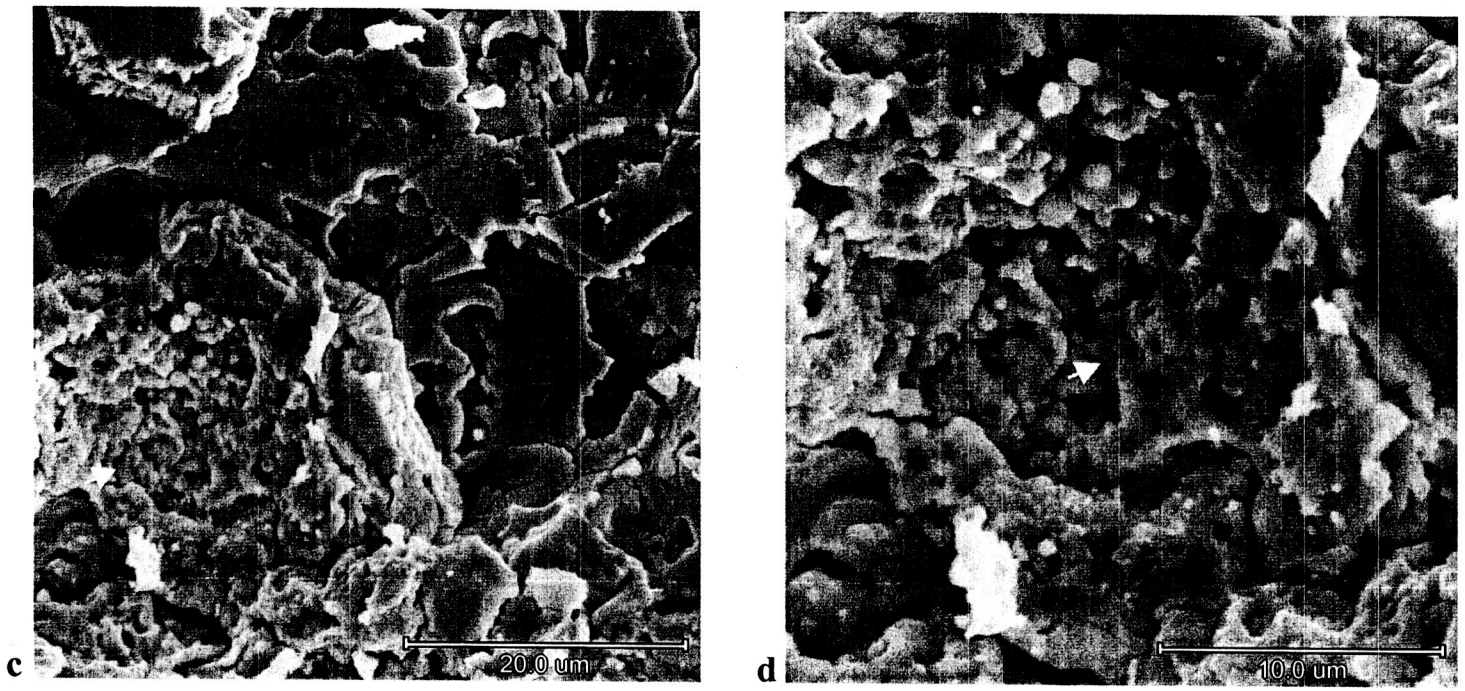

Figure 15 (cont.) (c) SEI image showing the irregular-shaped oxide structure on the top coat fracture surface of ADV-12. (d) Higher magnification of (c). White arrows indicate the irregular-shaped oxide, black arrows indicate smooth intersplat boundaries.

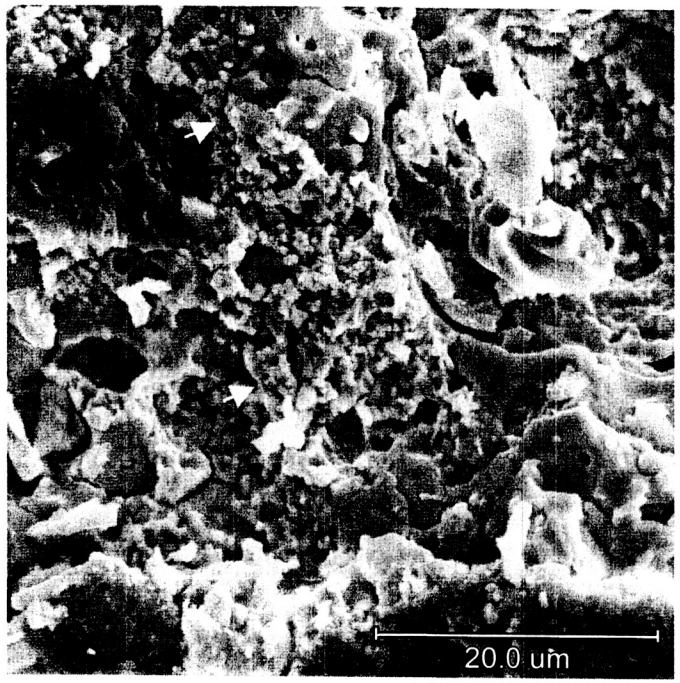

e

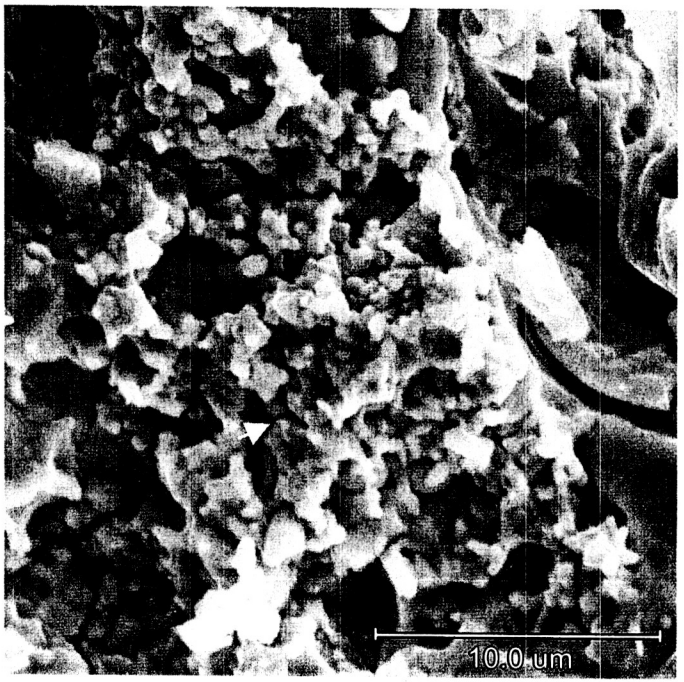

f

Figure 15 (cont.) (e) SEI image showing the irregular-shaped oxide structure on the top coat fracture surface of ADV-26B. (f) Higher magnification of (e). White arrows indicate the irregular-shaped oxide, black arrows indicate smooth intersplat boundaries.